

Spin-dependent electron impact ionisation of lithium from threshold to 80 eV

G Baum, E Kisker†, W Raith, W Schröder, U Sillmen and D Zenses
Universität Bielefeld, Fakultät für Physik, D-4800 Bielefeld, Federal Republic of Germany

Received 18 May 1981, in final form 13 July 1981

Abstract. The ionisation asymmetry is measured in a crossd-beam experiment utilising a W/EuS field emitter as a source of polarised electrons and dual-frequency optical pumping as the polarising process for the lithium atomic beam. The antiparallel-parallel asymmetry of the total ionisation cross section is positive with a broad maximum of 0.35 near threshold and a gradual decrease towards higher energies. A comparison is made with results of binary encounter and Born approximations. At threshold no significant variation of the asymmetry with energy is observed within a resolution of 0.3 eV.

1. Introduction

We report here the first results of an experiment measuring the asymmetry A of the total ionisation cross section of lithium for polarised electrons incident on polarised atoms. The asymmetry is defined as

$$A = \frac{\sigma(\uparrow\downarrow) - \sigma(\uparrow\uparrow)}{\sigma(\uparrow\downarrow) + \sigma(\uparrow\uparrow)} \quad (1)$$

where σ denotes the total ionisation cross section for the antiparallel and parallel spin configurations as indicated by the arrows. Asymmetry measurements provide additional information about the ionisation process, complementing absolute cross section data. For lithium, in the energy range from threshold to 100 eV, measurements of the asymmetry are particularly helpful for a better understanding of the ionisation process because the total ionisation cross section itself is not very well known in that energy range (cf Omidvar *et al* 1972). For other atoms similar asymmetry measurements have been performed on hydrogen by Alguard *et al* (1977) and on potassium by Hils and Kleinpoppen (1978). More recently a first preliminary value for sodium has been reported by Hils *et al* (1980).

The total ionisation cross section for unpolarised electrons, σ , can be expressed by the partial cross sections of the singlet (σ_1) and triplet (σ_3) states as

$$\sigma = \frac{1}{4}\sigma_1 + \frac{3}{4}\sigma_3. \quad (2)$$

For a parallel spin configuration of the incident particles the ionisation process is

† Present address: Institut für Festkörperforschung der Kernforschungsanlage Jülich, 5170 Jülich, Federal Republic of Germany.

described by σ_3 . For an antiparallel spin configuration, which is a mixture of singlet and triplet states, the expression $(\sigma_1/2 + \sigma_3/2)$ has to be used. The above defined asymmetry can therefore be expressed as

$$A = (\sigma_1 - \sigma_3)/4\sigma. \quad (3)$$

Thus A is a measure of singlet versus triplet ionisation events. Equivalently, one can discuss ionisation processes in terms of direct (σ_d) and exchange (σ_e) cross sections, connected to direct and exchange ionisation amplitudes (cf Rudge 1968). In this notation the unpolarised cross section is given by

$$\sigma = \sigma_d + \sigma_e - \sigma_{\text{int}} \quad (4)$$

where σ_{int} is related to the interference of direct and exchange amplitudes, caused by the indistinguishability of the two outgoing electrons in the case of parallel spins. For a parallel spin configuration of the incident particles one observes the quantity $(\sigma_d + \sigma_e - 2\sigma_{\text{int}})$, whereas for an antiparallel configuration one obtains $(\sigma_d + \sigma_e)$. The cross section asymmetry then becomes

$$A = \sigma_{\text{int}}/\sigma \quad (5)$$

and can be interpreted as a measure of the relative importance of interference effects in ionisation.

Peterkop (1961) pointed out that for impact ionisation the exchange amplitude is related to the direct amplitude and can be obtained from it. If spin-orbit effects are unimportant (as in case of Li) one has only two independent functions describing the ionisation process: (a) the absolute value of one of the amplitudes used in calculating $(\sigma_d + \sigma_e)$; (b) the relative phase between the amplitudes which determines the size of σ_{int} . By comparing equations (4) and (5) one sees that only if absolute cross section measurements are complemented by asymmetry measurements can both independent quantities be extracted separately.

Polarisation experiments are needed in many cases for a full understanding of collision problems in atomic physics. In the past technical problems and limitations of polarised sources and of polarimeters severely restricted such investigations. Recent progress in the development of polarised electron sources (cf Celotta and Pierce 1980, Baum 1981) and the availability of intense atomic beams, highly polarised by laser light, has given a new impetus to studies of spin-dependent effects in electron-atom collisions. The new information is often quite sensitive to details of the interaction.

2. Experimental method

A schematic diagram illustrating the experimental method for determining the ionisation cross section asymmetry is shown in figure 1. A beam of polarised Li atoms is crossed by a beam of polarised electrons. The ions formed in the collision region are extracted by a small electric field, further accelerated and focused onto a channel electron multiplier (CEM). The ion counting rate, N , is proportional to the ionisation cross section and, therefore, measurements of N for antiparallel and parallel orientation of the polarisation vectors allow the determination of the cross section

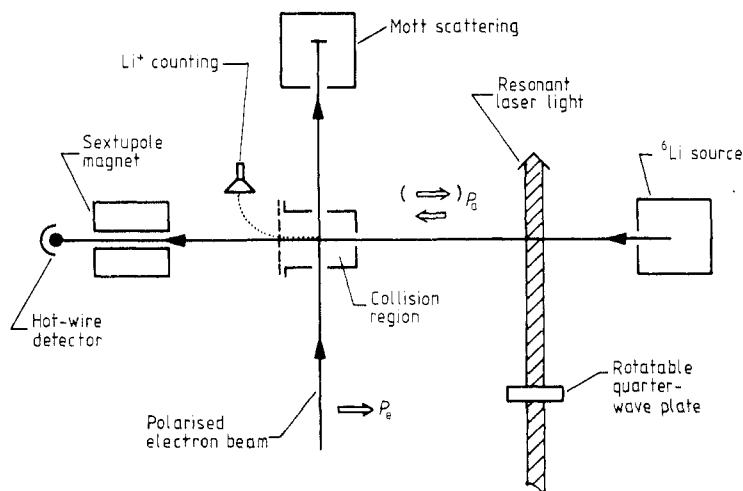


Figure 1. Schematic diagram of the experimental arrangement.

asymmetry A according to

$$A = \Delta / (P_e P_a) \quad (6)$$

with

$$\Delta = \frac{N(\uparrow\downarrow) - N(\uparrow\uparrow)}{N(\uparrow\downarrow) + N(\uparrow\uparrow)}. \quad (7)$$

P_e and P_a are the degrees of polarisation of the incident electron and atomic beams, respectively. They are measured separately.

In the collision region the atomic beam has a longitudinal polarisation, its direction determined by a small magnetic guiding field. The atomic polarisation is reversed by rotating the quarter-wave plate of the optical pumping system through 90° , without any changes in the magnetic guiding field. The polarisation of the electron beam is transverse with a large component, P_e , parallel to the atomic beam axis. The incident electron energy is determined by the potential of the metal enclosure surrounding the collision region. For data collection the incident electron energy is varied in steps over a selected energy range, going back and forth many times with a typical dwell time of 100 ms for each step. The polarisation of the atomic beam is reversed, alternating in a regular pattern uncorrelated to the energy dwell time, typically staying for a time of 3 s in one direction. The electron beam polarisation is kept constant during a run.

The ion counts are accumulated and stored according to incident energy and configuration of the beam polarisations. For each data recording channel the total accumulation time is determined by separately counting clock pulses. During a run the polarisations of the atomic and electron beams are measured repeatedly. The intensities of both beams are monitored continuously.

If necessary, the background resulting from ionisation of residual gas molecules is determined before and after each run by measurements with the atomic beam stopped in front of the collision region. A further correction is necessary as the atomic beam density in the collision region depends on the direction of the atomic beam polarisation. This instrumental effect is explained in § 4.

3. Apparatus

The layout of the polarised e-Li collision experiment is shown in figure 2. The crossed beams lie in the horizontal plane. Two major components of the apparatus are the polarised electron source and the polarised atomic beam system; both are discussed briefly at the beginning of this section.

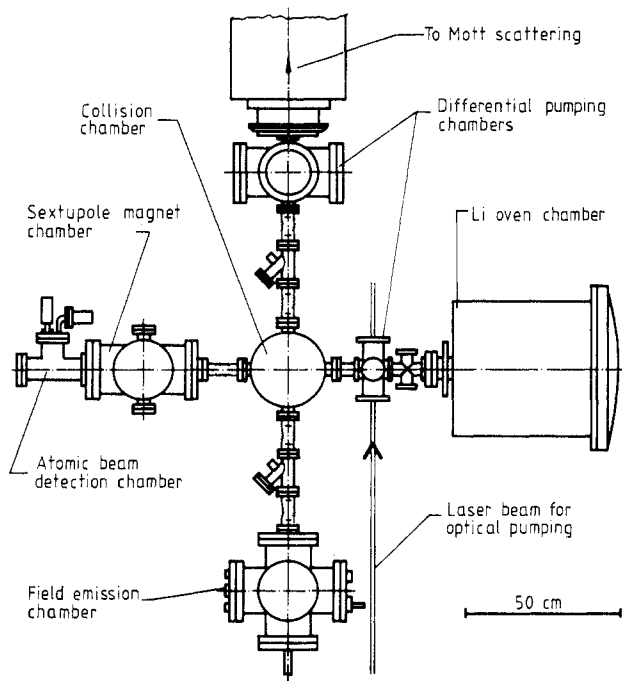


Figure 2. Layout of the apparatus.

The method employed for the production of polarised electrons is field emission from a tungsten tip covered with ferromagnetic EuS. A detailed description of the physical principles and characteristics of the source has been published previously (Baum *et al* 1977, Kisker *et al* 1978). Briefly, below the Curie temperature of EuS, electron tunnelling through the potential barrier at the internal W-EuS interface governs the emission process. Because of the ferromagnetic splitting of the EuS conduction band this internal field-emission process acts as a spin filter. In preparing a tip EuS is evaporated onto the clean $\langle 112 \rangle$ oriented tungsten tip and subsequently annealed to produce the characteristic emission behaviour when cooled to 10 K. Over a wide range of annealing conditions this emission current has a high transverse spin polarisation. A small magnetic field images the emission pattern onto a fluorescent screen and steering through an aperture (probe hole) selects a certain spot for polarisation analysis, energy-distribution measurements, and collision studies. The direction of the polarisation in the transverse plane cannot be predicted in advance. However, it is found that each tip possesses preferred axes (presumably the crystallographic directions of each magnetisation) to which the spin is always parallel or

antiparallel. Usually it is no problem to find a spot which has a large polarisation component parallel to the atomic beam axis. One can also rotate the spin direction through about $\pm 45^\circ$ in azimuth by changing the magnitude of the imaging magnetic field. The direction and magnitude of the polarisation are measured in a Mott scattering apparatus after acceleration to 100 keV. Four semiconductor detectors are mounted symmetrically for 120° backward scattering with an azimuthal spacing of 90° . From studies of the foil-thickness dependence of the Mott asymmetry it was determined that the theoretical analysing power of 0.39 for an infinitesimally thick target was reduced by 10% for the 31 nm gold foil. The vertical component of the Earth's magnetic field is compensated over the entire electron beam line. The horizontal component of the Earth's field (about $10 \mu\text{T}$) is parallel to the beam line.

The energy distribution of the electron beam depends very critically on the annealing conditions. For measuring the electron energy distribution by the method of retarding-field analysis a Faraday cup can be moved onto the beam axis directly behind the probe hole. In this experiment we usually had an energy width of $\Delta E \approx 0.6\text{--}1 \text{ eV}$; for threshold measurements we worked with narrower energy distributions ($\Delta E \leq 0.3 \text{ eV}$). The total emission current is kept below $3 \times 10^{-8} \text{ A}$, as otherwise the emission tends to become unstable in the course of a run, exhibiting current oscillations.

The lithium-6 atomic beam is spin polarised by optical pumping with circularly polarised resonance light. The method and the polarised atomic beam system have recently been described in detail (Baum *et al* 1980). The lithium atomic beam is produced by effusion from an oven orifice. We used 95% enriched lithium-6. The construction and the operation of the oven and collimator are very similar to the atomic beam system described by Alguard *et al* (1979). The beam divergence is kept below 0.01 rad by collimation. On its way to the collision chamber the beam is crossed with circularly polarised laser light which originates from a single-mode dye laser, pumped by a cw Ar ion laser. The light is tuned to the $2S_{1/2}\text{--}2P_{3/2}$ transition. Simultaneous pumping of both hyperfine ground states is achieved with the help of an acousto-optic modulator, which generates a second laser light beam. The two light beams differ in frequency by the operating frequency of the modulator which is set to 228 MHz, corresponding to the lithium-6 HFS splitting. Through repeated cycles of absorption and spontaneous emission the atoms are orientated with their spins pointing parallel (antiparallel) to the direction of the pumping light beam if σ^+ (σ^-) circularly polarised light is used. Thus by rotating the quarter-wave plate through 90° the atomic beam polarisation is reversed in direction.

A small magnetic field of 0.7 mT, parallel to the light beam, is applied in the pumping region. The spin direction adiabatically follows the magnetic field direction which turns through 90° in space until it is longitudinal to the atomic beam at the entrance of the collision chamber. This longitudinal guiding field is reduced in strength to $10 \mu\text{T}$ in the centre of the collision chamber. The field strength increases again between collision chamber and sextupole magnet.

The sextupole magnet is employed as polarisation analyser for the atomic beam. The magnet is strong enough to be considered as a perfect high-field state selector with an analysing power of unity. It consists of three sections each of 7.6 cm length, 0.32 cm central bore diameter and about 0.9 T pole-tip field. Behind the sextupole magnet a hot-wire detector measures the intensity of the high-field state-selected beam containing atoms characterised by the quantum numbers $F = 3/2$; $m_F = 3/2, 1/2$ and $-1/2$. Sequential measurements of I^- , the atomic beam intensity for σ^- pumping, I^+ , the beam intensity for σ^+ pumping, and I^0 , the intensity with the pumping light turned off,

allow a determination of the polarisation (Baum *et al* 1980). The atomic beam polarisation, P_a , is typically 0.7[†].

The atomic beam density in the collision region is estimated to be $n = 5 \times 10^9 \text{ cm}^{-3}$ at an oven temperature of 1050 K. The orifice temperature is kept 100 K higher in order to reduce the dimer content (Li_2) of the beam. This reduction was confirmed directly by observing the fluorescent intensity of molecular transitions excited by laser light. Thermodynamic calculations are in agreement with our experimental estimate for the fraction of dimers in the beam (less than 1%).

A detailed drawing of the components inside the collision chamber is shown in figure 3. The chamber is evacuated by a turbomolecular pump which maintains a residual gas

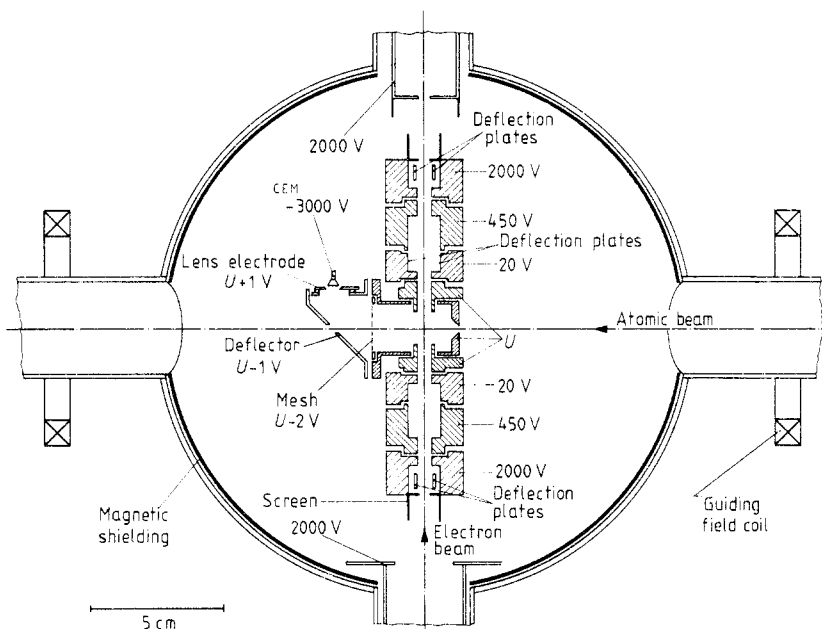


Figure 3. Top-view scale drawing of the collision chamber showing the deceleration and acceleration electron optics as well as the ion collection arrangement. The collision energy is determined by the voltage U . Typical electric potentials of the electron-optical elements are indicated. The deflection plates are in each case orthogonal pairs.

pressure of 10^{-9} Torr under operating conditions. All parts surrounding the collision region are gold plated to insure a uniform contact potential. The entrance collimator of 0.3 cm diameter for the atomic beam prevents deposition of lithium on these surfaces.

[†] In carrying out this experiment we made attempts to bring the atomic polarisation closer to unity (see Baum *et al* 1980 for some proposed measures), but were unsuccessful. Only recently we learned about the effect of coherent population trapping (Gray *et al* 1978) which can be of importance in optical pumping if two frequencies couple to a common upper level, as is the case in our atomic polarisation scheme. Estimates of the percentage of coherently trapped atoms in levels with low electronic polarisation and the existence of some phenomena in the optical pumping, which would not be explained satisfactorily in the past, strongly indicate that this effect is indeed non-negligible under our experimental conditions and can easily explain why a higher atomic polarisation cannot be obtained.

The magnetic shielding consists of a 1 mm thick sheet of magnetically soft iron. It extends 30 cm above and below the cross section plane shown in figure 3. The magnetic field at the centre of the guiding-field coils is about 2 mT. The electron beam is transported at an energy of 2 keV to the collision chamber with the field-emission tip being at ground potential. The deceleration and acceleration electron optics were adapted from a design of Kuyatt and Plummer (1972). For additional information electron trajectories through this system have been calculated with a computer program (Fink and Kisker 1980). The lenses are made of a special austenitic Ni-Cr stainless steel (german steel classification 1.3952). The smallest electron beam aperture has a diameter of 0.3 cm.

The Li^+ ions produced pass through a gold-plated copper mesh (cf figure 3) which is at a lower potential ($U - 2$ V) than the surroundings of the interaction region (U). The extraction field influences only slightly the potential at the centre of the collision region, causing a decrease in the potential by less than 1% of the extraction voltage. This was experimentally confirmed in observing the displacement of the onset of ionisation with 15 V applied to the mesh electrode. A deflector bends the ion trajectories towards the CEM where some focusing can be achieved with the additional lens electrode. We estimated the collection efficiency to be close to unity.

A microprocessor board (Kim I) is used for controlling the annealing temperature of the field-emission tip and for accumulating the Mott-scattering data. A second microprocessor board (Kim I) is used for controlling the dye-laser operation, with programs for etalon and cavity stabilisation, frequency scan and quarter-wave plate rotation. The signals used for optimising the laser performance are the atomic beam intensities beyond the sextupole magnet[†], we aim to minimise I^- and to maximise I^+ . A microprocessor board (Z80 CPU, 16k RAM) is used for multichannel scaling, electron beam energy ramping and data recording. A background program allows on-line display of relevant parameters such as electron beam polarisation, atomic beam polarisation, ion counting rate asymmetry and statistical counting errors. The cross section asymmetry can be computed off-line from the data records stored on digital cassettes.

The experimental operation starts with fine adjustment of the dye-laser system while the lithium oven is heated up. It is easy to find the 2S-2P resonance lines using the frequency scan program. About five hours are needed for adjusting optical components in order to get a well polarised atomic beam, which is then stable for about ten hours. In this ionisation experiment it was not necessary to run the atomic beam at full intensity. A 100 g load of lithium-6 lasted for several hundred hours of beam time. After the electron optics and the data acquisition system have been checked and adjusted with unpolarised electrons from the tungsten tip, the W/EuS emitter is prepared and cooled down with liquid helium. If the characteristics of the field-emission current are unsatisfactory for the intended run a new EuS layer is prepared in a short time. Runs typically last for half an hour. The consumption of liquid helium is about 3 l h^{-1} . The dye solution must be replaced every 20 h of accumulated running time to maintain good operating conditions in the wavelength region of 670 nm.

Typical performance parameters for data collection are listed in table 1.

[†] In our first runs the laser was stabilised by using the near-resonance birefringence of the polarised beam (cf Baum *et al* 1980). Later on the hot-wire signal was taken for frequency stabilisation as this was technically simpler to do. By proper adjustments of the optical system, under conditions where a small magnetic field is present in the pumping region, we made certain that the extrema of the I^+ and I^- hot-wire signals occurred at the same frequency.

Table 1. Characteristic parameters of the polarised electron source, polarised atomic beam and ion asymmetry measurement.

(i) <i>Polarised electrons</i>	
Method	Field emission
Polarisation (transverse)	0.8
Effective component, P_e	≈ 0.6
Current	10 nA
Minimum energy spread (FWHM)	0.3 eV
(ii) <i>Polarised atoms</i>	
Method	Optical pumping
Polarisation, P_a	0.7
Polarisation reversal	Optical
Density	$5 \times 10^9 \text{ cm}^{-3}$
Dimer fraction	< 0.01
(iii) <i>Ion asymmetry measurement</i>	
Ionisation cross section at 10 eV (max)	$\approx 3 \times 10^{-16} \text{ cm}^2$
Fraction of background contribution	
5.4–18 eV	< 0.01
18–80 eV	0.01 to 0.3
Counting rate (max)	10 kHz
Raw asymmetry, Δ (max)	0.15
$P_e P_a$	0.45
Instrumental effects	≈ 0.07

4. Results

The results of the measured cross section asymmetry A are shown in figure 4. The data are a combination of many runs covering various energy ranges and having different electron polarisation directions. The energy resolution is $\Delta E(\text{FWHM}) = 0.3 \text{ eV}$ near threshold. For larger incident energies the data have been averaged over the energy intervals specified in the figure caption. The energy scale is calibrated by observing the onset of ionisation and is considered to be accurate to within 0.1 eV. This calibration is consistent with the zero point of the energy scale as determined from retarding potential measurements.

Above an incident energy of 18 eV a correction must be made for background contributions due to ionisation of residual gas molecules. This background rate was, in the worst case, 30% of the Li^+ signal. A further correction is necessary because the atomic beam density in the collision region depends slightly on polarisation, being n_+ (n_-) for a polarisation which is parallel (antiparallel) to the magnetic guiding field. Null-asymmetry checks with unpolarised electrons showed that the density asymmetry δ , which is defined as $\delta = (n_+ - n_-)/(n_+ + n_-)$, depends on the magnitude of P_a and on the strength of the magnetic field in the pumping region.

The observed density asymmetry can be understood in the following way: momentum-transfers in repeated photon absorption processes bend the paths of the atoms in the optical pumping region. This effect is not cancelled by the recoil in spontaneous photon re-emission as the emission process is not unidirectional. The frequencies of the optical pumping transitions differ slightly for σ^+ and σ^- pumping because of the Zeeman splitting of the ground and excited state HFS levels. The frequencies of the laser for σ^+ and σ^- pumping are the same, which is assured through the optical

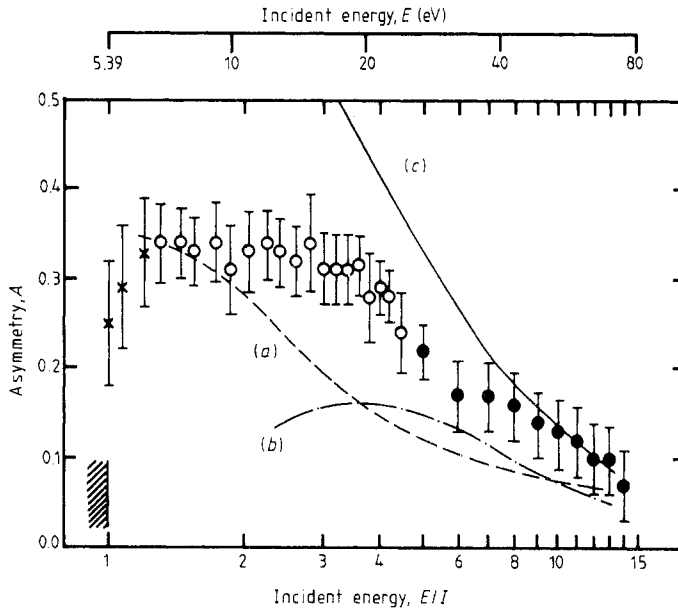


Figure 4. Impact ionisation asymmetry A plotted against electron energy E , in units of the threshold energy $I = 5.39$ eV. \times , measurements with energy resolution of $\Delta E(\text{FWHM}) = 0.3$ eV; \circ , measurements with energy resolution of $\Delta E \sim 1$ eV; \bullet , measurements averaged over a 5 eV range. Error bars are discussed in the text. The data are compared with theoretical predictions based upon the following approximations: (a) binary encounter formulae of Vriens (1966); (b) Born exchange (Peach 1966); (c) Ochkur (Peach 1966).

adjustment process. The linewidth of the laser is smaller than the Doppler width of the atomic beam. With the given divergence of the atomic beam and the associated Doppler shift, the central part of the 'resonance region' for σ^+ light has a geometric location which is slightly different from that for σ^- light. The different locations together with the atom-trajectory bending at the pumping zone (about 0.5 mrad for 10 absorbed photons per atom) lead to different atomic beam profiles for σ^+ and σ^- light downstream from the zone. An aperture of diameter 0.3 cm right in front of the collision region (see figure 3), located 27 cm downstream from the pumping zone, selects part of the profile and gives rise to a polarisation-dependent density of the atomic beam at the intersection with the electron beam. For strong pumping light, leading to a high atomic beam polarisation, this effect is more pronounced than for weak pumping light. For most runs the $2S_{1/2}-2P_{3/2}$ resonance line has been used for optical pumping. Later experience showed that the $2S_{1/2}-2P_{1/2}$ transition would have introduced smaller systematic errors because of two effects: (a) the Zeeman splitting of the $2P_{1/2}$ level is six times smaller than that of the $2P_{3/2}$ level; (b) atoms in the $2S_{1/2}$, $m_F = +3/2$ ($-3/2$) state are unaffected by σ^+ (σ^-) laser light tuned to the $2S_{1/2}-2P_{1/2}$ transition.

To correct for the density asymmetry effect the counting rate asymmetry Δ (see equation (7)) is obtained from the raw counting rate asymmetry Δ' by

$$\Delta = (\Delta' \pm \delta) / (1 \pm \Delta' \delta) \approx \Delta' \pm \delta. \quad (8)$$

The upper (lower) sign applies if the electron beam polarisation is parallel (antiparallel) to the magnetic guiding field. For high atomic polarisations δ had values of up to 0.07.

Quantitative estimates, based on the explanation given above, are in agreement with the size of this correction. Contributions to ionisation events from Li_2 are neglected, as the Li_2 concentration in the beam is small (see § 3) and no signal is seen in the energy range from 5.0–5.4 eV where only Li_2 could be ionised.

The size of most of the error bars is dominated by systematic effects. Uncertainty in the correction of the atomic beam density asymmetry contributes about as much as the errors in the beam polarisations of P_e and P_a . In addition, the error bars include scatter of the results for the numerous runs, thus accounting to some extent for unknown systematic errors. For the three data points near threshold the error is dominated by counting statistics.

5. Discussion

For lithium there is little theoretical work with which to compare our measurements. In the following we apply the formulae of the binary encounter model (Vriens 1966) to lithium ionisation and discuss the results of Peach (1966), derived with the Born exchange as well as the Ochkur approximation.

The binary encounter model (Vriens 1966) treats the ionisation processes mainly through momentum and energy transfer in the free electron–electron collision. The electron binding is taken into consideration by an isotropic momentum distribution of the valence electron and by a gain in kinetic energy of the incident electron in the Coulomb field of the atom, prior to the collision. Curve (a) in figure 4 was calculated using equation (4) from this paper and equations (24) and (26) from Vriens' paper with the terms interpreted properly. The kinetic energy of the target electron at the moment of collision, E_2 , was taken to be the value for which the radial charge distribution has a maximum ($E_2 = 3.7$ eV; $r_{\text{max}} = 3a_0$). For other hydrogen-like atoms this model, similarly applied, predicts maximum values of the asymmetry of 0.3 for hydrogen and 0.4 for potassium. The measurements on these atoms, however, yielded maximum values of 0.5 for hydrogen (Alguard *et al* 1977) and 0.2 for potassium (Hils and Kleinpoppen 1978).

Other assumptions in the quantitative evaluation of the binary encounter model for lithium are possible. If for E_2 the average over all radial distances ($E_2 = 5$ eV) is taken, the calculated asymmetry values lie below curve (a) of figure 4. If ϕ'' (see equation (24) of Vriens 1966) is approximated by unity, the asymmetry results with $E_2 = 3.7$ eV are generally larger by about 0.1 than the measured values, whereas with $E_2 = 5$ eV reasonable agreement with the data can be obtained. The above approximation for ϕ'' , however, is well justified only if the electron energy at the moment of collision is much larger than the Rydberg energy.

The binary encounter model is well suited for understanding qualitatively the sign and shape of the cross section asymmetry by relating it to the free electron–electron (Møller) scattering asymmetry. Bincer (1957) gives the dependence of this asymmetry on the relative kinetic energy transfer $w = W/E'$, where W is the energy lost in the collision and E' is the kinetic energy of the incident electron at the moment of collision. The free electron–electron asymmetry, defined in accordance with equation (1), is always positive, and for $w = \frac{1}{2}$ equal to unity. It approaches zero if w tends either toward zero or unity. At threshold one gets a free electron–electron scattering asymmetry of 0.75 with $w = I/(E + 2I)$. For $E/I = 2$ the relative energy transfer can lie between $w = 0.27$ and 0.54, having a range in asymmetry from 0.42 to 0.9. A broad

shoulder of the asymmetry can be expected around this energy value. On average for higher incident energies smaller fractions of energy are transferred and A therefore decreases.

The main method for calculating ionisation processes is the Born approximation. This approximation is considered to be reliable only at energies above five to ten times threshold energy. For lithium the only calculations available which include exchange are those of Peach (1966), presenting results based on the Born exchange and the Ochkur approximation. As the full range Born approximation cross section, $\sigma' = \sigma_d + \sigma_e$, is also given, one can extract the interference cross section and calculate A ,

$$A = (\sigma' - \sigma) / \sigma \quad (9)$$

using for σ either the Born exchange or the Ochkur results. The asymmetry obtained with Born exchange results (figure 4(b)) lies below the experimental data. The asymmetry is sensitive to the phase between direct and exchange ionisation amplitudes. In the theoretical treatment a value of the phase has to be chosen judiciously. For hydrogen, numerous Born exchange results are available. They show large variations, depending on the choice of the phase. For potassium no exchange calculations have been performed. The Ochkur approximation results (curve (c)) seem to overestimate the size of the cross section asymmetry. The same holds for the corresponding situation in hydrogen (see curve (j) in figure 2 of Alguard *et al* 1978). The 'modified' Born results of Peach (1966), which arbitrarily exclude exchange effects and yield $\sigma = \sigma_d$, i.e. $\sigma_e = \sigma_{\text{int}}$ (cf equation (4)), can also be used to calculate an asymmetry from equation (9). This asymmetry (not shown in figure 4) happens to be in better agreement with our data than the approximations which explicitly include exchange.

6. Threshold behaviour

The energy dependence of the asymmetry near threshold deserves special attention as this experiment is the first of its kind to probe the threshold region with a narrow electron energy distribution. Our asymmetry data show only a small variation in approaching the ionisation limit. This behaviour implies a very similar dependence on energy for the singlet and triplet cross sections (cf equation (3)). If the Wannier-Peterkop-Rau threshold law (see Fano 1980 and references therein) is valid and only S states contribute, the asymmetry should rise to $A = +1$ near threshold. This is contradictory to our data at an energy resolution of 0.3 eV.

The threshold behaviour of the asymmetry depends on the occurrence of nodes or antinodes of the two-electron wavefunction at the Wannier saddle position, which follow from symmetry considerations. The threshold law supposedly reads $\sigma \propto (E - I)^{3.881}$ in the presence of nodes on the saddle and $\sigma \propto (E - I)^{1.127}$ if nodes are absent (Klar 1980). For S waves the parity is even and therefore the appearance of an antinode or node is correlated with the singlet or triplet character. This is not the case for partial waves of higher total angular momentum as they can be of either parity. There is no fundamental reason why the total orbital angular momentum vanishes at energies a finite amount above threshold. If P states contribute, then a ^3P wavefunction can have an antinode near the saddle[†], allowing this triplet state to have a threshold

[†] As Klar (1981) confirmed, there is a misprint in the paper of Klar and Schlecht (1976) which implied that the nodal character depends on the spin only and that near threshold ionisation into triplet states always gives much smaller cross sections ($\sigma \propto (E - I)^{3.881}$) than ionisation into singlet states ($\sigma \propto (E - I)^{1.127}$).

behaviour similar to the (singlet) 1S state. Thus our lithium asymmetry data near threshold suggest that, at a resolution of 0.3 eV, either non-zero angular momentum states (P or higher) contribute significantly to the ionisation process, or the Wannier-Peterkop-Rau threshold law is valid only at energies closer to threshold.

7. Summary

Our measurement of the spin dependence in the impact ionisation of lithium by electrons provides a better understanding of this ionisation process. The ionisation asymmetry gives information about the interference of the direct and exchange amplitudes, about which nothing was previously known experimentally for lithium. Near threshold, singlet and triplet cross sections behave similarly with energies which leads to conclusions about the range of validity of the threshold law and the character of contributing wavefunctions.

Acknowledgments

We are grateful to Dr C D Caldwell for important contributions in the early stage of this research. We thank one of our referees for bringing the effect of coherent population trapping to our attention. This work has been supported in part by the State of Nordrhein-Westfalen under project FA 7894.

References

- Alguard M J, Clendenin J E, Ehrlich R D, Hughes V W, Ladish J S, Lubell M S, Schüler K P, Baum G, Raith W, Miller R H and Lysenko W 1979 *Nucl. Instrum. Meth.* **71** 29–59
- Alguard M J, Hughes V W, Lubell M S and Wainwright P F 1977 *Phys. Rev. Lett.* **39** 334–8
- Baum G 1981 *Polarization Phenomena in Nuclear Physics* (AIP Conf. Proc. No 69) ed G G Ohlsen (New York: American Institute of Physics) pp 785–96
- Baum G, Caldwell C D and Schröder W 1980 *Appl. Phys.* **21** 121–6
- Baum G, Kisker E, Mahan A H, Raith W and Reihl B 1977 *Appl. Phys.* **14** 149–53
- Bincer A M 1957 *Phys. Rev.* **107** 1434–8
- Celotta R J and Pierce D T 1980 *Advances in Atomic and Molecular Physics* vol 16 (New York: Academic) pp 101–57
- Fano U 1980 *Phys. Rev. A* **22** 2660–71
- Fink J and Kisker E 1980 *Rev. Sci. Instrum.* **51** 918–20
- Gray H R, Whitley R M and Stroud C R Jr 1978 *Opt. Lett.* **3** 218–20
- Hils D and Kleinpoppen H 1978 *J. Phys. B: At. Mol. Phys.* **11** L283
- Hils D, Rubin K and Kleinpoppen H 1980 *Coherence and Correlation in Atomic Collisions* ed H Kleinpoppen and J F Williams (New York: Plenum) 689–96
- Kisker E, Baum G, Mahan A H, Raith W and Reihl B 1978 *Phys. Rev. B* **18** 2256–75
- Klar H 1980 *Coherence and Correlation in Atomic Collisions* ed H Kleinpoppen and J F Williams (New York: Plenum) 67–77
- 1981 private communication
- Klar H and Schlecht W 1976 *J. Phys. B: At. Mol. Phys.* **9** 1699–711
- Kuyatt C E and Plummer E W 1972 *Rev. Sci. Instrum.* **43** 108–11
- Omidvar K, Kyle H L and Sullivan E C 1972 *Phys. Rev. A* **5** 1174–87
- Peach G 1966 *Proc. Phys. Soc.* **87** 381–91
- Peterkop R K 1961 *Proc. Phys. Soc. A* **77** 1220–2
- Rudge M R H 1968 *Rev. Mod. Phys.* **40** 564–90
- Vriens L 1966 *Proc. Phys. Soc.* **89** 13–21